Plasma Phys. Control. Fusion **41** (1999) 551–565. Printed in the UK PII: S0741-3335(99)98379-3

Non-axisymmetric simulation of the vertical displacement event in tokamaks

Young Yun Lim, Jae Koo Lee, Kyo Jin Shin and Min Sup Hur

Department of Physics, Pohang University of Science and Technology, Pohang 790-784, South Korea

Received 12 May 1998, in final form 13 January 1999

Abstract. Tokamak plasmas with highly elongated cross sections are subject to a vertical displacement event (VDE). The nonlinear magnetohydrodynamic (MHD) evolutions of tokamak plasmas during the VDE are simulated by a three-dimensional MHD code as a combination of $N = 0$ and $N = 1$ components. The nonlinear evolution during the VDE is strongly affected by the relative amplitude of the $N = 1$ to the $N = 0$ modes.

1. Introduction

The tokamak [1] is a toroidal confinement system with the plasma confined by a magnetic field. The need for high β and high plasma currents demands a vertically elongated plasma, which is inherently unstable to vertical displacements. During such an event, the vacuum vessel may be subject to large vertical forces and the observed distribution of the halo current is not toroidally axisymmetric [2]. Most of the previous studies are carried out assuming an axisymmetry in the toroidal direction, which is thus inadequate for explaining the non-axisymmetry of the experimental observation. The tool employed in the present study to simulate a vertical displacement event (VDE) with three-dimensional non-axisymmetry is a magnetohydrodynamic (MHD) simulation code CART [3, 4] that can be used to calculate the time development of the MHD instability and equilibrium of the plasma during the event [5, 6].

The fluctuating quantities of plasma instability are represented as $F(r, \theta, \phi) = f(r) \exp[\mathrm{i}(m\theta + N\phi)]$ where N is the toroidal mode number and m the poloidal mode number. The $N = 0$ vertical mode alone is sufficient to trigger the vertical motion of the plasma current. Varying amplitudes of the $N = 1$ non-axisymmetric mode, relative to the $N = 0$ axi-symmetric mode as initial perturbations, are included to elucidate the role of the non-axisymmetric component in the nonlinear evolution of the vertical instability arising from the tokamak non-circularity and the high current with finite pressure and resistivity in a free boundary.

In section 2.1, free boundary equilibria are described. The three-dimensional MHD program CART is described briefly in section 2.2. In section 3.1, the linear properties of $N = 0$ and $N = 1$ are examined. In section 3.2 the nonlinear simulation of the $N = 0$ vertical instability alone is shown and in section 3.3 that of the $N = 0$ mode mixed with the $N = 1$ mode is simulated by varying the ratio of the $N = 0$ mode to the $N = 1$ mode.

0741-3335/99/040551+15$19.50

2. Simulation method

2.1. FBT program for tokamak equilibrium

The tokamak model used in this paper has 14 poloidal current coils and two quadrupole current coils which are positioned at a vertically symmetric position in figure 1, with major radius $R_{\text{major}} = 1.4$ m and plasma radius $R_{\text{minor}} = 0.25$ m. The modelled tokamak has two up–down symmetric divertors with inverse aspect ratio $\epsilon = R_{\text{minor}}/R_{\text{major}} = 0.18$ and a rectangular wall boundary. To satisfy the boundary conditions at the wall where $\hat{n} \cdot \vec{B} = \hat{n} \cdot \vec{V} = 0$, the perturbed poloidal magnetic flux function A, the perturbed velocity stream function U and the perturbed plasma pressure P are set to vanish: $A_N = U_N = P_N = 0$ ($N = 0, 1, 2, \ldots$).

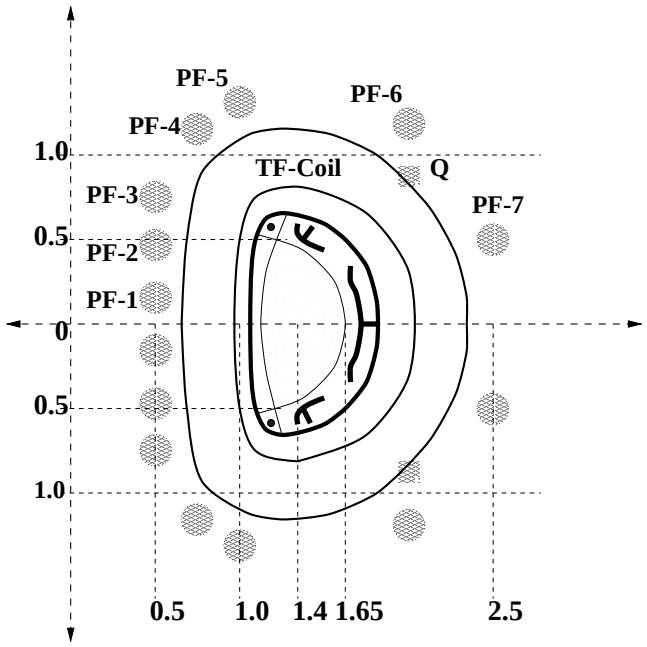

Figure 1. The high-pressure and high-current elongated tokamak model.

Given the coil distribution, reference MHD equilibria are computed using the free boundary MHD equilibrium code FBT [5] which calculates highly elongated and arbitrarily shaped equilibria with separatrices and multiple magnetic axes. The plasma shape is chosen to have elongation $\kappa = 2.0$, to allow for adequate vertical stabilization [7].

We employ two different equilibria (Ga) and (Na). The state of the equilibrium state function (Ga) in figure 2 is for a plasma horizontal radius 0.25 m, a plasma vertical radius 0.5 m, a plasma elongation $\kappa = 2.0$, a toroidal vacuum magnetic field $B_{\text{tor}} = 3.5$ T, a toroidal plasma current $I_{\text{plasma}} = 0.51$ MA, a plasma peak pressure 1.37×10^4 Pa, a plasma $\beta_{\text{toroidal}} = 0.06\%$, a plasma $\beta_{\text{poloidal}} = 7.8\%$ and a safety factor q at 95% of the flux surface $q_{95} = 3.8$. The state of the equilibrium state function (Na) is for a toroidal magnetic field $B_{\text{tor}} = 2.5$ T, a toroidal plasma current $I_{\text{plasma}} = 0.37$ MA, a plasma peak pressure 1.78×10^4 Pa, a plasma $\beta_{\text{toroidal}} = 0.16\%$, a plasma $\beta_{\text{poloidal}} = 20\%$ and $q_{95} = 3.7$. Both equilibria have a q-value on the axis of 1.01 and a triangularity of 0.5 as in [6]. The profile forms, as functions of the poloidal flux function, are the same for the two equilibria employed in our simulation. As shown in figure 2(d), the pressure gradient just inside the last closed flux surface is very

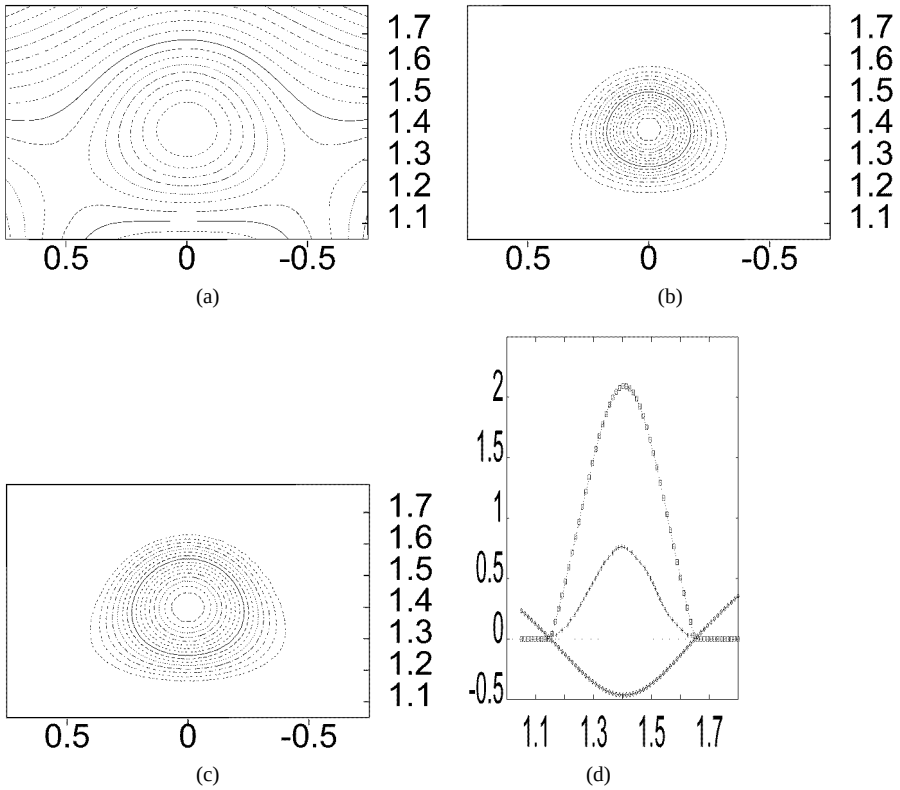

Figure 2. The plasma equilibrium function (Ga) for (a) the poloidal magnetic flux function A, (b) the plasma pressure P, (c) the toroidal plasma current J_ϕ, (d) the profiles of A (diamond symbols), P (+ symbols enhanced by 100) and J_ϕ (squares) along $Z = 0$.

small. We have used an equilibrium from the commonly used code FBT [5] (not the force-free equilibrium) which has a smaller pressure gradient than the current gradient.

The passive plates, the shaped vacuum vessel and the TF coils shown in figure 1 are not included in our simulation. The plasma equilibrium functions calculated by FBT are used as the initial state for the CART program.

2.2. CART algorithm

The equations used in this paper are the tokamak resistive MHD equations [8, 9]. The coordinates used here are the (R, Z, ϕ) Cartesian coordinates and the spectral representation in the toroidal direction has been used. The direction of $\hat{\phi}$ is defined as $\hat{R} \times \hat{Z} = \hat{\phi}$.

The equations are as in [10]:

$$\left(\frac{\partial}{\partial t} + \vec{V}_\perp \cdot \nabla_\perp - \frac{2}{R_0}\frac{\partial U}{\partial Z}\right) W = \vec{B}_\perp \cdot \nabla_\perp J_\phi + \frac{2}{R_0}(\hat{R} \times \nabla_\perp P) \cdot \hat{\phi} + \mu \nabla^\dagger W \tag{1}$$

$$\frac{\partial A}{\partial t} = -\vec{V}_\perp \cdot \nabla_\perp A + \frac{\vec{B}_\phi}{R_0}\frac{\partial U}{\partial \phi} + \eta J_\phi \tag{2}$$

$$\frac{\partial P}{\partial t} = -\vec{V}_\perp \cdot \nabla_\perp P + \kappa_\perp \nabla_\perp{}^2 P \tag{3}$$

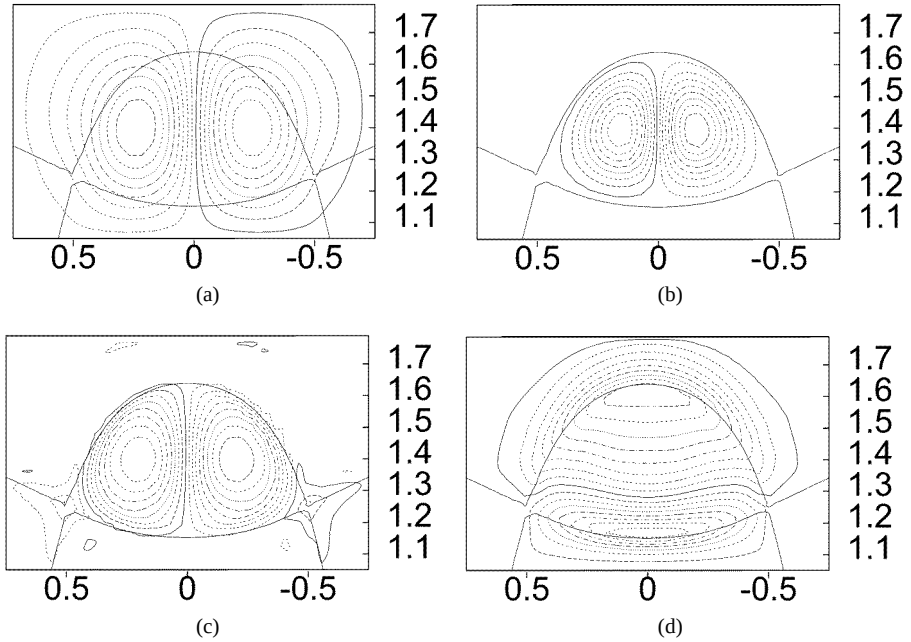

Figure 3. The $N = 0$ linear perturbation function for (a) the poloidal magnetic flux function A, (b) the plasma pressure P, (c) the toroidal plasma current J_ϕ, (d) the poloidal velocity stream function U.

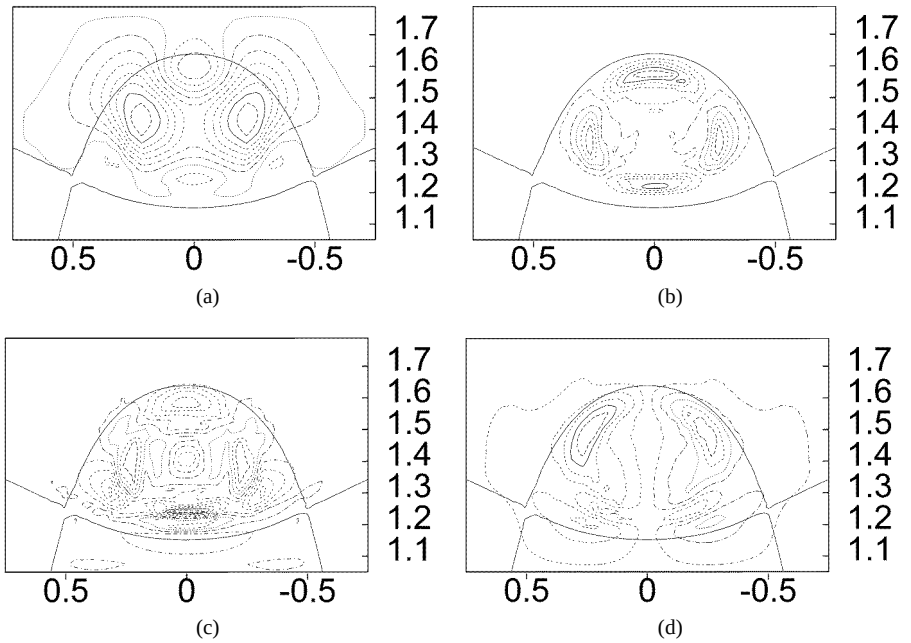

Figure 4. The $N = 1$ linear perturbation function for (a) the poloidal magnetic flux function A, (b) the plasma pressure P, (c) the toroidal plasma current J_ϕ, (d) the poloidal velocity stream function U.

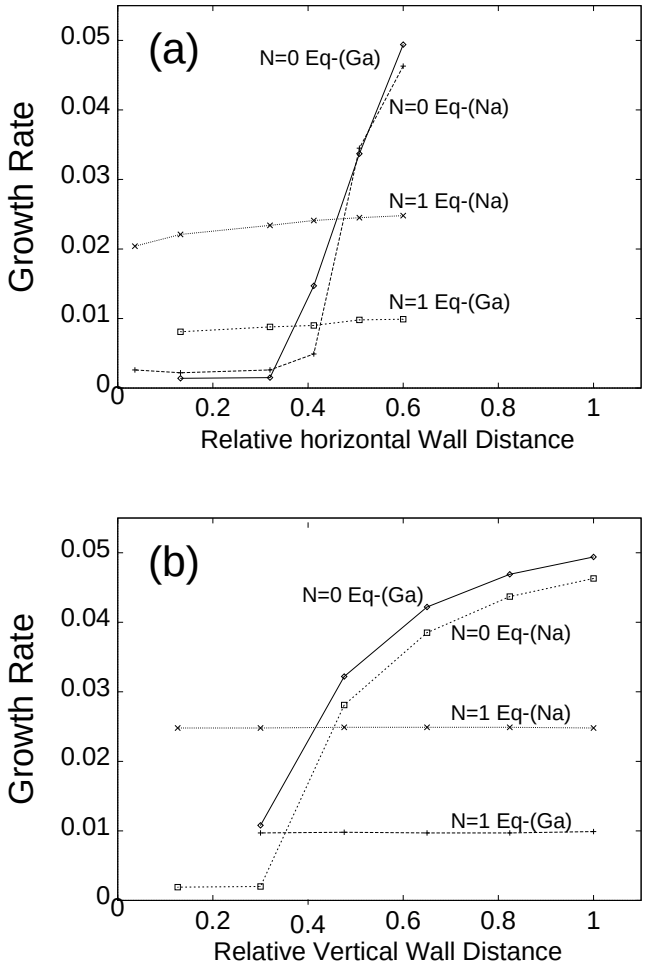

Figure 5. Linear growth rate against various wall positions: (a) horizontal wall position and (b) vertical wall position.

where

$$\vec{V}_\perp = \frac{R}{R_0}\nabla_\perp U \times \hat{\phi} \tag{4}$$

$$\vec{B}_\perp = \frac{R_0}{R}\nabla_\perp A \times \hat{\phi}. \tag{5}$$

Here, R_0 stands for the centre location of the computational domain, $\kappa_\perp$ for thermal conductivity (a constant in our simulation), μ for viscosity and η for resistivity. A is the $\hat{\phi}$ component of $\vec{A}$ where $\vec{B} = \nabla \times \vec{A}$. The equation for the pressure P is an energy equation including both convection and conduction. The toroidal plasma current J_ϕ is calculated by

$$J_\phi = {\nabla_\perp}^2 A - \frac{1}{R}\frac{\partial A}{\partial R}. \tag{6}$$

The operator $\nabla^\dagger$ is defined as

$$W = \nabla^\dagger U = {\nabla_\perp}^2 U + \frac{1}{R}\frac{\partial U}{\partial R}. \tag{7}$$

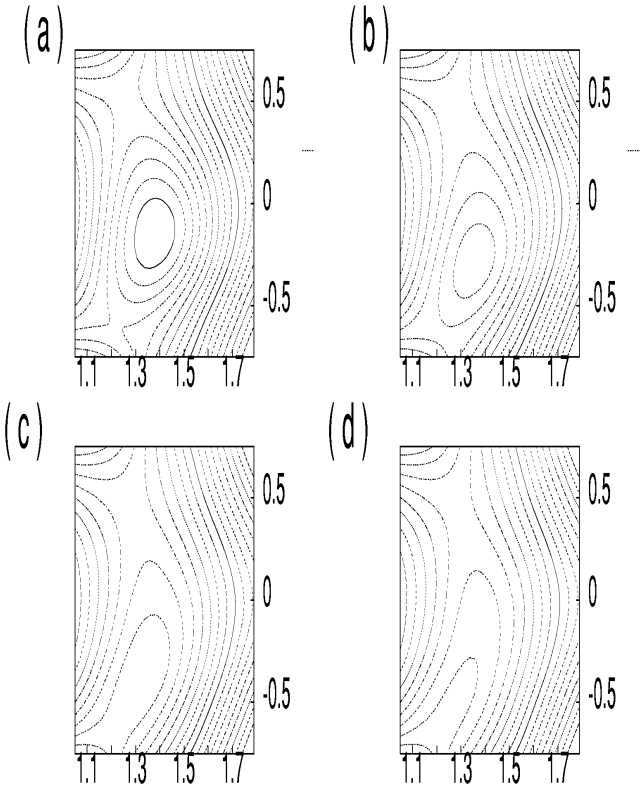

Figure 6. The $N = 0$ nonlinear poloidal magnetic stream function A at times of (a) 0.734 ms, (b) 1.100 ms, (c) 1.467 ms, (d) 1.834 ms.

In the linear mode, the equations are linearized about the equilibrium and the perturbation solution is iterated in time for each harmonic N until it grows with an exponential time dependence $e^{\gamma t}$. In the nonlinear mode, the linear eigenfunctions are used to initialize the nonlinear evolutions. Several N modes are coupled and the full nonlinear equations are iterated in time until the predetermined number of timesteps is reached.

The variables are time-iterated with a two-step Lax Wendroff scheme

$$\psi^{t+\frac{1}{2}\Delta t} = \psi^t + \tfrac{1}{2}\Delta t f(\psi^t) \qquad \text{(half step)}$$

$$\psi^{t+\Delta t} = \psi^t + \Delta t f(\psi^{t+\frac{1}{2}\Delta t}) \qquad \text{(full step)}.$$

The diffusive terms of the form $\tau\nabla_\perp^2\psi$ are treated explicitly over several subcycles $\delta t = \Delta t/K$

$$\psi^{t+\delta t} = \psi^t + (\delta t)\tau\nabla_\perp^2\psi$$

where K is typically larger than 10. The explicit time step has a von Neumann condition of the form

$$\delta t \leqslant \frac{(\Delta r)^2}{\tau}$$

where Δr is the mesh size.

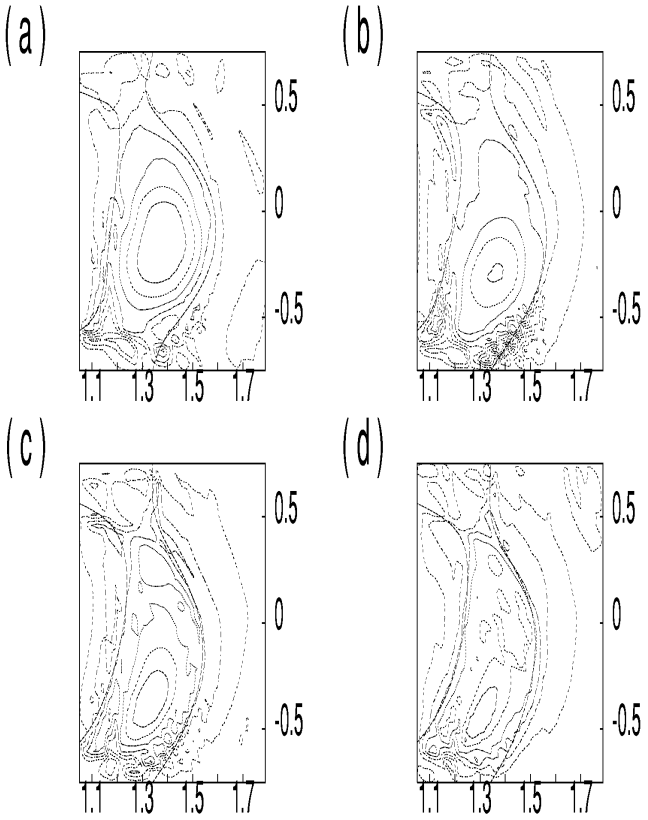

Figure 7. The $N = 0$ nonlinear toroidal plasma current J_ϕ at times of (a) 0.734 ms, (b) 1.100 ms, (c) 1.467 ms, (d) 1.834 ms.

Plasma resistivity η is $1/\tau_\gamma\omega_A$, where τ_γ is resistive diffusion time owing to plasma resistivity and $\omega_A = V_A/R_p = (q_0/R_0B_{tor})(\mu_0 m_p n_p)^{1/2}$ is the poloidal Alfvén frequency and V_A the poloidal Alfvén velocity. The normalized time step $dt = 0.01$ in the CART-program is the time scale with the Alfvén time to be 1.0. During the simulation, the resistivity in the plasma centre is 10^{-4} and the uniform resistivity in the vacuum region is 10^{-2}. In the plasma area, the resistivity is inversely proportional to J_ϕ. The plasma viscosity μ is 10^{-4} uniformly. 65 grids are used in both the directions of R and Z.

3. Simulation results

3.1. Linear eigenmode interaction with conducting wall

Linear perturbation functions calculated from the equilibrium function (Ga) and (Na) are investigated. The growth rates of the linear perturbation functions depend on the tokamak wall position both vertically or horizontally. The figures of the equilibrium functions are shown in the case of equilibrium (Ga) in figure 2. The figures of the equilibrium (Na) are similar to equilibrium (Ga) and therefore omitted.

The wall distance is from the plasma boundary; thus the wall distance 0.6 means that the straight conducting walls are at a location 0.6 times the plasma minor radius measured from the

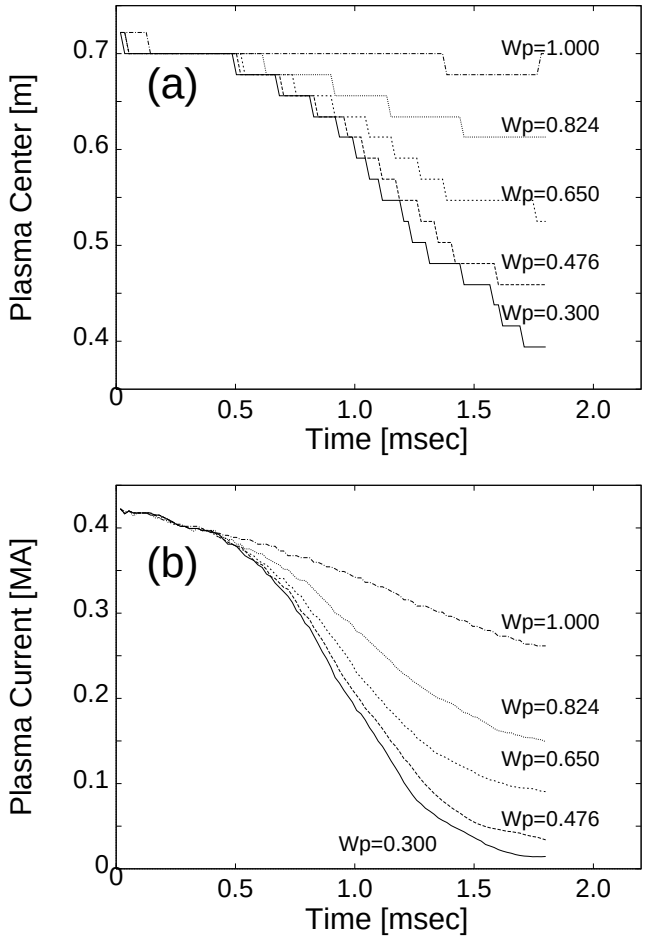

Figure 8. $N = 0$ axisymmetric nonlinear evolution for various wall positions W_p for the time evolution of (a) the vertical motion of the plasma centre Z_{mag} and (b) the toroidal plasma current.

plasma boundary. All the perturbed quantities vanish at the ideally conducting boundary wall which is shaped conforming to the rectangular shape of our computational domain. The only walls are the ideally conducting straight walls at the specified wall locations. The equilibrium is not self-consistently recalculated as the plasma evolves nonlinearly, thus showing a substantial downward motion; the simulation shows a short time evolution resulting from instabilities with $N = 0$ (vertical) and $N = 1$ (resistive external and internal pressure and current-driven kink).

The $m = 1$ mode structure is observed from figures 3 and 4. The linear eigenmode, unstable for the given equilibrium, is obtained in (E, Z) meshes independent of the initial trial perturbation. In fact, the code CART does not employ the Fourier mode expansion in the poloidal direction (it only does so in the toroidal direction), so that the linear eigenmodes found in the code are the results of the physical instability pattern at small amplitudes, naturally exhibiting the $m = 1$ mode. Which lobes in figures 3 and 4 are positive or negative is not relevant for the linear eigenmodes in these initial value codes. The $m = 1$ linear perturbation function indicates the vertical displacement of the tokamak plasma. The perturbation of the magnetic field and the plasma current make a force $\vec{F} = \vec{J} \times \vec{B}$. This

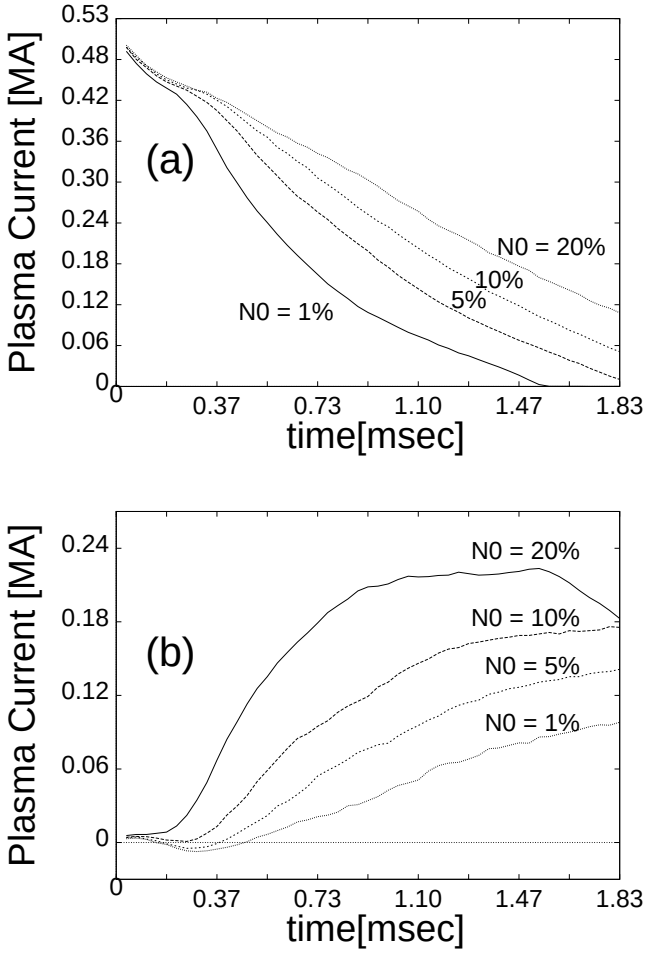

Figure 9. Nonlinear simulations with only the $N = 0$ perturbation: (a) the toroidal plasma current with varying initial perturbations of the $N = 0$ mode and (b) the scrape-off-layer current with varying $N = 0$ initial perturbations.

force is the vertical instability that makes the plasma move down to the lower part of the tokamak.

The $N = 1$ linear perturbation functions show the poloidal mode $m = 2$ as in figure 4. The linear growth rates of the $N = 0$ mode and $N = 1$ mode are shown in figure 5. The $N = 0$ linear growth rate is strongly dependent on the wall distance. Because of the toroidal magnetic field effect, the growth rate of the equilibrium (Ga) is smaller than the equilibrium (Na). The $N = 0$ instability can be stabilized by the tokamak wall distance and the $N = 1$ instability by the toroidal magnetic field [11].

3.2. Nonlinear simulation of $N = 0$ mode

In the nonlinear simulation with the $N = 0$ mode only, the equilibrium function evaluated in the FBT code and the linear perturbation function evaluated in the linear simulation are

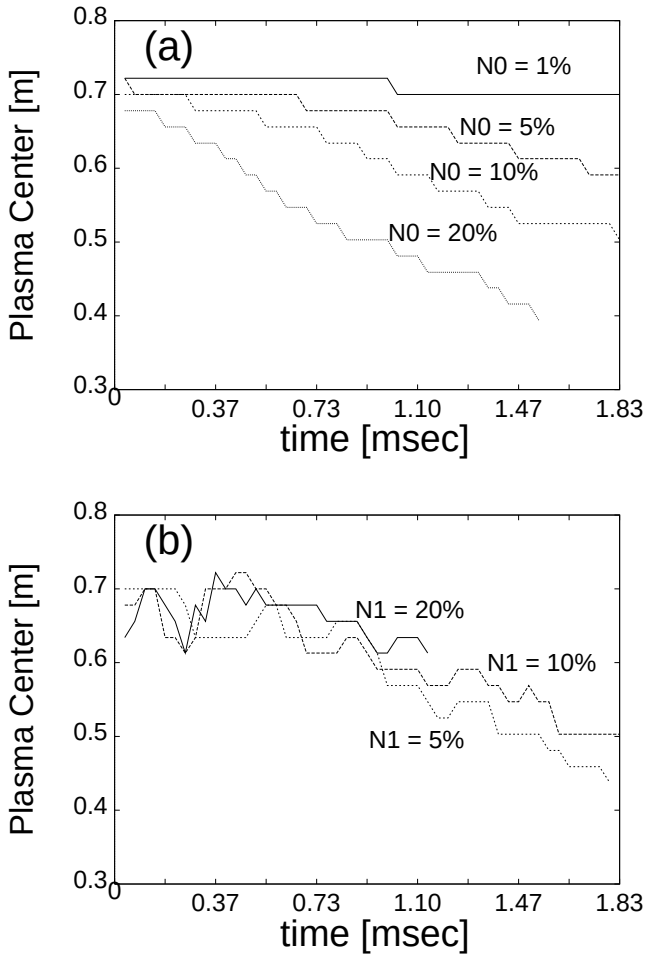

Figure 10. The magnetic axis displacement (a) with varying $N = 0$ perturbations when the $N = 1$ perturbation is fixed at 1% and (b) with varying $N = 1$ initial perturbations when the $N = 0$ perturbation is fixed at 10%.

used as initial values and full nonlinear equations are iterated. The magnitude of the linear perturbation function ranges from 10% to 1% of the magnitude of the equilibrium.

Because the time evolutions of the equilibrium (Ga) and (Na) are very similar, that of the equilibrium (Ga) is shown here. The horizontal wall distance is set to be [1:0.6, R_{minor}:wall distance] and the vertical wall distance is set to be [1:0.5]. As shown by figure 6, the plasma moves vertically downward. In figure 7, the plasma current shows a similar feature as the poloidal magnetic stream function A [12].

Our simulations start from the linear eigenmodes with $N = 0$ and $N = 1$ (with variable relative starting amplitudes) to observe a nonlinear state exhibiting a substantial displacement of the plasma centre. $N = 2$ and $N = 3$ are indicated as the first and the second nonlinear harmonics, respectively, growing from these linear ($N = 0$ and $N = 1$) eigenmodes. It is believed that the general nature of the nonlinear evolution does not change qualitatively from the present results with small mode numbers in the case when a simulation is carried out with fairly large number of N modes.

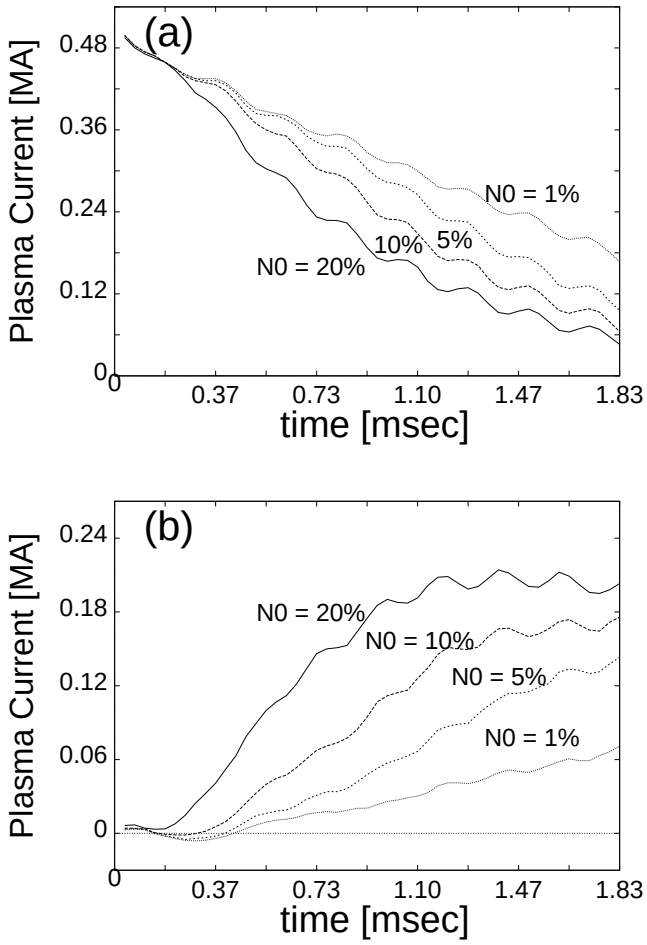

Figure 11. Varying $N = 0$ initial perturbations when the $N = 1$ perturbation is fixed at 1% for (a) the toroidal plasma current and (b) the scrape-off-layer current.

The vertical displacement of the plasma magnetic axis is calculated for various positions of the vertical wall. The relation between the magnetic axis movement and the tokamak wall distance is shown in figure 8(a). As shown in figure 8(a), the magnetic axis movement is weakened when the wall approaches the plasma. Also, the decay of the plasma current shows a feature similar to the magnetic axis movement in figure 8(b). The decay of the toroidal plasma current decreases when the wall approaches the plasma. These results are consistent with those of the previous analysis when the $N = 0$ instability can be stabilized by a tokamak wall. The vertical displacement is associated with the large force originating from the interactions between the poloidal magnetic field and the halo currents which flow into the tokamak vessel from the tokamak plasma, $\vec{F} = \vec{J_\psi} \times \vec{B_{\rm pol}}$ [13, 14]. The quantized (stepwise) motion of the plasma centre is related to the finite mesh size, so that this motion can be smoothed to a finer scale in the case when a fine mesh is employed.

Figure 9 shows the decay of the plasma current and the growth of the scrape-off-layer current for the case when the $N = 1$ perturbation is not added to the equilibrium and the $N = 0$ perturbation is varied. The scrape-off current is defined as the total plasma current

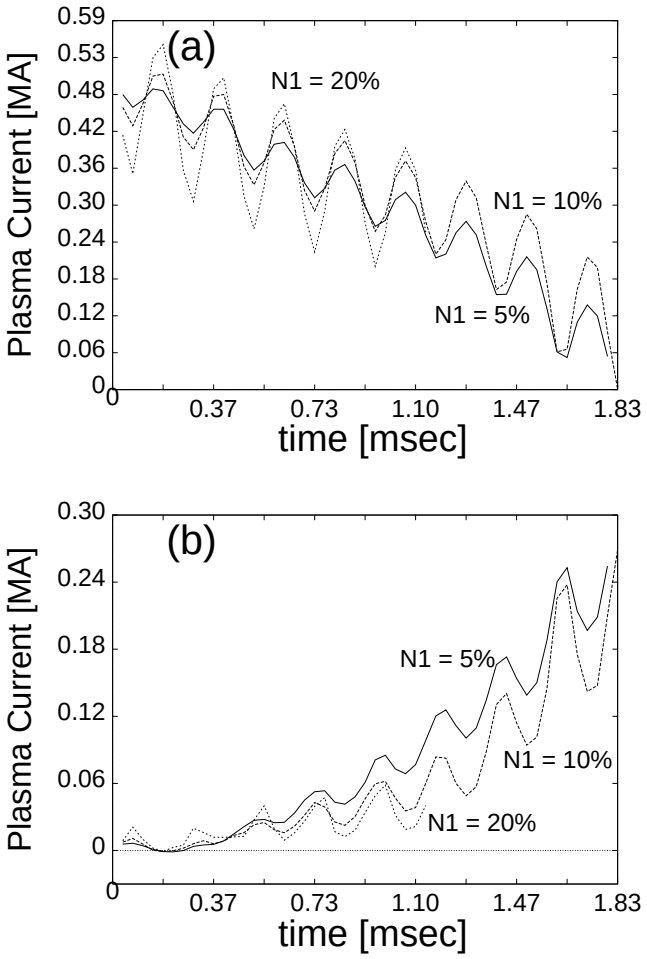

Figure 12. Varying $N = 1$ initial perturbations when the $N = 0$ perturbation is fixed at 10% for (a) the toroidal plasma current and (b) the scrape-off-layer current.

outside the last magnetic separatrix with an x-point which is changing in time as the plasma moves downwards because of the vertical displacement instability in figure 8. The scrape-off current is calculated as the lost plasma current as the plasma centre moves downwards in time. As the plasma evolves in time, we first calculate the plasma current at a fixed location ($R = 1.24$ and $Z = -0.5$) same as the original lower x-point of the equilibrium as in figure 2(a) or figure 3 (the separatrix) and subtract this portion from the original total plasma current in the equilibrium to identify it as the scrape-off current.

3.3. $N = 0$ and $N = 1$ mixing

In the previous section, the linear simulation of the $N = 0$ mode alone during the VDE has been studied. However, there have been experimental observations that the comparable magnitude of the $N = 1$ mode is mixed with the $N = 0$ mode during the VDE [2]. The simulation of mixed $N = 0$ and $N = 1$ modes can give some physical insight into the understanding of the VDE. Various ratios of $N = 0$ to $N = 1$ are used in our nonlinear simulations.

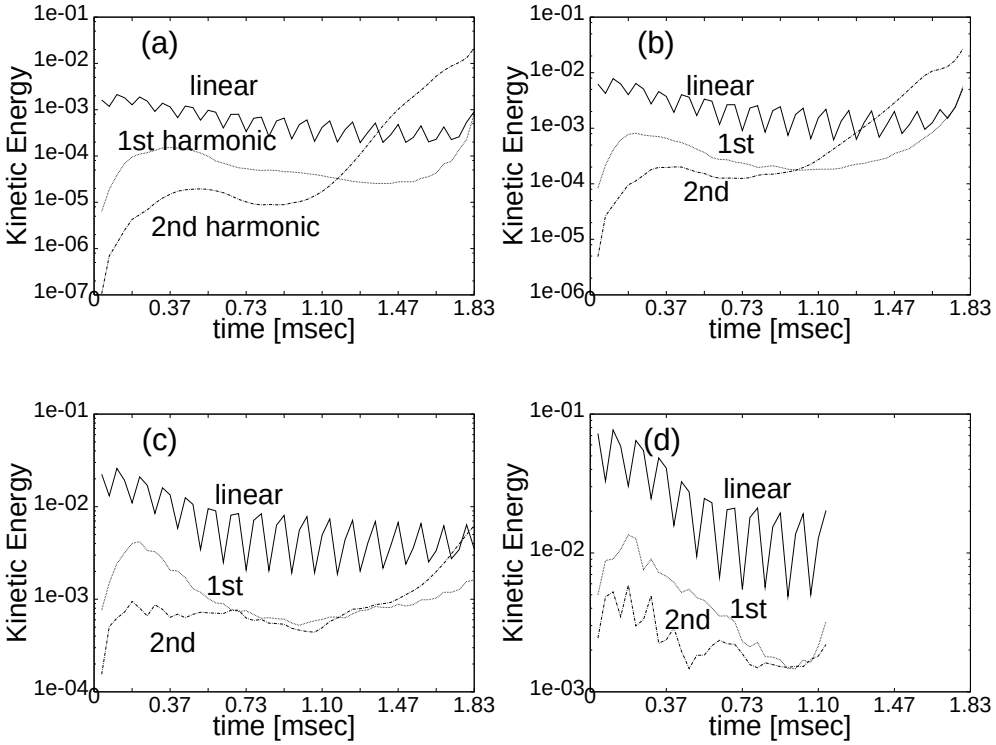

Figure 13. Time evolution of the $N = 0$ linear and harmonic components of the kinetic energy when the $N = 1$ perturbation is fixed at 1% for the $N = 0$ perturbation of (a) 1%, (b) 5%, (c) 10%, (d) 20%.

In figure 10(a), the $N = 1$ perturbation is fixed at 1% of the equilibrium amplitude and the $N = 0$ perturbation is varied. Almost the same results are obtained as for the $N = 0$ mode alone because of the small amplitude of $N = 1$. Very different features start to appear in figure 10(b) where the $N = 0$ perturbation is fixed at 10% of the equilibrium and the $N = 1$ perturbation is varied from 5 to 20%. It can be seen that the displacement of the magnetic axis is gradually suppressed as the amplitude of $N = 1$ mode becomes larger.

Figure 11 shows the decay of the plasma current and the growth of the scrape-off-layer current for the case when $N = 1$ is fixed at 1% of the equilibrium amplitude and $N = 0$ is varied. Small oscillations of current are seen originating from the $N = 1$ mode. These oscillations are somewhat related to the finite mesh size. The scrape-off-layer current is the current that is scraped off the divertor before triggering a halo current [15]. In figure 11 the toroidal plasma current decreases at a faster rate and the scrape-off-layer current increases at a faster rate when the $N = 0$ perturbation becomes larger. Therefore, the $N = 0$ mode promotes the VDE.

In figure 12, the amplitude of the $N = 1$ initial perturbation is varied with a fixed $N = 0$ amplitude, where the oscillation of the current becomes intense because of the larger amplitude of the $N = 1$ mode. The toroidal plasma current decreases at a slower rate and the scrape-off-layer current increases at a slower rate when the $N = 1$ perturbation becomes larger. The time evolution of the kinetic energy is investigated in figure 13. The growth of the $N = 0$ second harmonic becomes steeper as the initial amplitude of the $N = 0$ linear perturbation

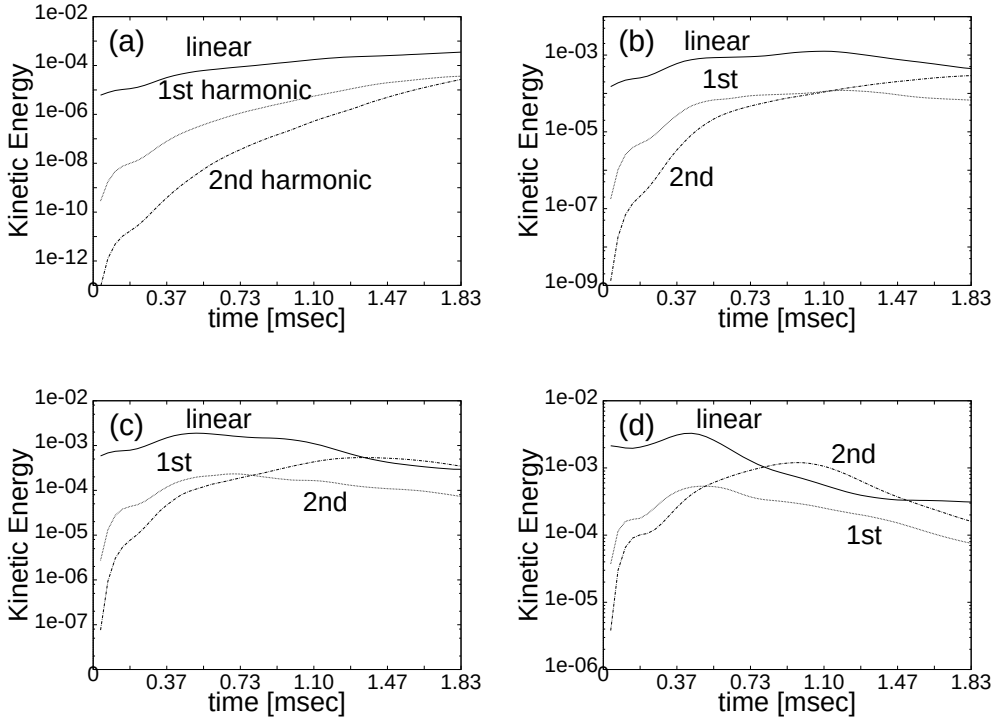

Figure 14. Time evolution of the $N = 1$ linear and harmonic components of the kinetic energy when the $N = 0$ perturbation is fixed at 10% for the $N = 1$ perturbation of (a) 2.5%, (b) 5%, (c) 10%, (d) 20%.

becomes larger. The $N = 0$ mode promotes the second harmonic of the kinetic energy, related to the fast vertical disruption of the plasma. The time evolution of the kinetic energy of the $N = 1$ mode shows a different feature. In figure 14, the growth of the second harmonic of the $N = 1$ kinetic energy becomes weakened as the amplitude of the $N = 1$ mode becomes larger. The $N = 1$ mode tends to suppress the growth of the second harmonic. Future studies should include more toroidal modes such as the $N = 2$, $N = 3$, and others. The present study is focused on the inclusion of a non-axisymmetric mode, in particular $N = 1$ (which is the most important non-axisymmetric mode).

4. Summary and conclusion

Finite-pressure and high-current non-circular tokamak equilibria are calculated by the FBT program to be used in linear and nonlinear resistive MHD simulations by the CART code. The vertical displacement of the plasma results from $N = 0$ alone. Varying proportions of the $N = 1$ mode, included along with the $N = 0$ mode, elucidate the physical phenomena and the consequences of the instability which is initiated by an axisymmetric instability and evolves to a non-axisymmetric instability. No prior non-axisymmetric simulation has been carried out on this aspect of the VDE despite the experimental observation of a significant amplitude of non-axisymmetry. The $N = 0$ mode promotes the growth of the second harmonic of the kinetic energy and the $N = 1$ mode reduces its growth.

Acknowledgments

Helpful discussions with Dr Y B Kim, Dr M S Chu and Dr T S Taylor are gratefully acknowledged. The present studies were supported (in part) by the Basic Science Research Institute Program, Ministry of Education 1998, Project No BSRI 98-2439.

References

[1] Wesson J A 1978 *Nucl. Fusion* **18** 87
[2] Granetz R S, Hutchinson I H, Sorci J and Irby J H 1996 *Nucl. Fusion* **36** 545
[3] Lee J K 1986 *Nucl. Fusion* **26** 955
[4] Lee J K 1986 *Phys. Fluids* **29** 1629
[5] Hofmann F *et al* 1987 *Nucl. Fusion* **27** 743
[6] Kim S K *et al* 1995 *Fusion Technol.* **27** (S) 436
[7] Marcus F B *et al* 1990 *Nucl. Fusion* **30** 1511
[8] Strauss H R 1977 *Phys. Fluids* **20** 1354
[9] Izzo R *et al* 1983 *Phys. Fluids* **26** 2240
[10] Lee J K, Strait E J, Lao L L and Taylor T S 1989 *Nucl. Fusion* **29** 1181
[11] Freidberg J P and Haas E A 1973 *Phys. Fluids* **16** 1909
[12] Lao L L and Jensen T H 1991 *Nucl. Fusion* **31** 1909
[13] Jensen T H and Skinner D G 1990 *Phys. Fluids* B **2** 2358
[14] Nakamura Y *et al* 1996 *Nucl. Fusion* **36** 295
[15] Gruber O *et al* 1993 *Plasma Phys. Control. Fusion* **35** B191